Geol. Mag. **154** (*2*), *2017, pp. 247–264.* © *Cambridge University Press 2016*
doi:10.1017/S0016756815001065

Lower Wenlock black shales in the northern Holy Cross Mountains, Poland: sedimentary and geochemical controls on the Ireviken Event in a deep marine setting

JUSTYNA SMOLAREK*, WIESŁAW TRELA‡, DAVID P. G. BOND§ & LESZEK MARYNOWSKI*¶†

*Faculty of Earth Sciences, University of Silesia, Będzińska 60, 41–200 Sosnowiec, Poland
‡The Polish Geological Institute – National Research Institute, Zgoda 21, 25–953 Kielce, Poland
§Department of Geography, Environment and Earth Sciences, University of Hull, Cottingham Road, Hull, HU6 7RX, United Kingdom
¶Wrocław Research Centre EIT + Ltd, Stabłowicka 147, 54–066 Wrocław, Poland

(*Received* 21 February 2015; *accepted* 23 November 2015; *first published online* 4 February 2016)

Abstract – The stratigraphic variability and geochemistry of Llandovery/Wenlock (L/W) Series boundary sediments in Poland reveals that hemipelagic sedimentation under an anoxic/euxinic water column was interrupted by low-density bottom currents or detached diluted turbid layers that resulted in intermittent seafloor oxygenation. Total organic carbon values and inorganic proxies throughout the Wilków 1 borehole section suggest variable redox conditions. U/Mo ratios > 1 throughout much of the Aeronian and Telychian stages, together with an absence of pyrite framboids, suggest oxygenated conditions prevailed. However, elevated total organic carbon near the Aeronian/Telychian boundary, together with increased U/Th and V/(V + Ni) ratios and populations of small pyrite framboids are consistent with the development of dysoxic/anoxic conditions at that time. U/Th, V/Cr and V/(V + Ni) ratios, as well as U_{authig} and Mo concentrations, suggest that during the Ireviken black shale deposition, bottom-water conditions deteriorated from oxic during Telychian time to mostly suboxic/anoxic immediately prior to the L/W boundary, before a brief reoxygenation at the end of the Ireviken black shale sedimentation in the Sheinwoodian Stage. Rapid fluctuations in U/Mo during the Ireviken Event are characteristic of fluctuating redox conditions that culminated in an anoxic/euxinic seafloor in Sheinwoodian time. Following Ireviken black shale deposition, conditions once again became oxygen deficient with the development of a euxinic zone in the water column. The Aeronian to Sheinwoodian deep-water redox history was unstable, and rapid fluctuations of the chemocline across the L/W Series boundary probably contributed to the Ireviken Event extinctions, which affected mainly pelagic and hemipelagic fauna.

Keywords: Ireviken Event, redox conditions, inorganic proxies, pyrite framboids, Silurian.

1. Introduction

The Ireviken Event (IE) records a little-studied, but important, Silurian extinction at the Llandovery/Wenlock (L/W) Series boundary (Telychian/Sheinwoodian Stage boundary) (e.g. Calner, 2008). Extinction losses began at the base of the Lower *Pseudooneotodus bicornis* conodont Zone and culminated during the Lower *Kockelella ranuliformis* Zone (e.g. Lehnert *et al*. 2010). The observed carbon and oxygen isotopic excursions began considerably later, but might share their origins with extinctions, through feedbacks in the carbon and oxygen system. Munnecke, Samtleben & Bickert (2003) suggested that the anoxia responsible for the extinction losses originated in the deep oceans, before invading the shallower shelf seas. The IE scarcely affected shallow-water reefs, while pelagic and hemipelagic organisms such as the graptolites, conodonts and trilobites suffered preferential losses (Calner, 2008).

†Author for correspondence: leszek.marynowski@us.edu.pl

Until now, the reconstruction of palaeoenvironments during the IE has been based on stable carbon and oxygen isotope studies (Munnecke, Samtleben & Bickert, 2003; Cramer & Saltzman, 2005, 2007; Noble *et al*. 2005; Loydell & Frýda, 2007; Lehnert *et al*. 2010; Vandenbroucke *et al*. 2013), but interpretations have not always been consistent with other sedimentological and geochemical observations (e.g. Page *et al*. 2007). Some palaeoceanographic models infer permanent anoxia in the pycnocline (Wilde, Barry & Quinby-Hunt, 1991; Bickert *et al*. 1997), while other authors propose cold, oxic bottom-water regimes during deposition of Silurian sediments (Jeppsson, 1990). Major discrepancies exist in proposed sea-level histories (see compilations in Munnecke *et al*. 2010; Melchin, Sadler & Cramer, 2012) and in the origins of redox changes (Jeppsson, 1990; Bickert *et al*. 1997; Page *et al*. 2007).

Most knowledge of the IE derives from much better exposed shallow-shelf settings (e.g. Munnecke, Samtleben & Bickert, 2003; Lehnert *et al*. 2010; Racki *et al*. 2012). Here we investigate palaeoredox

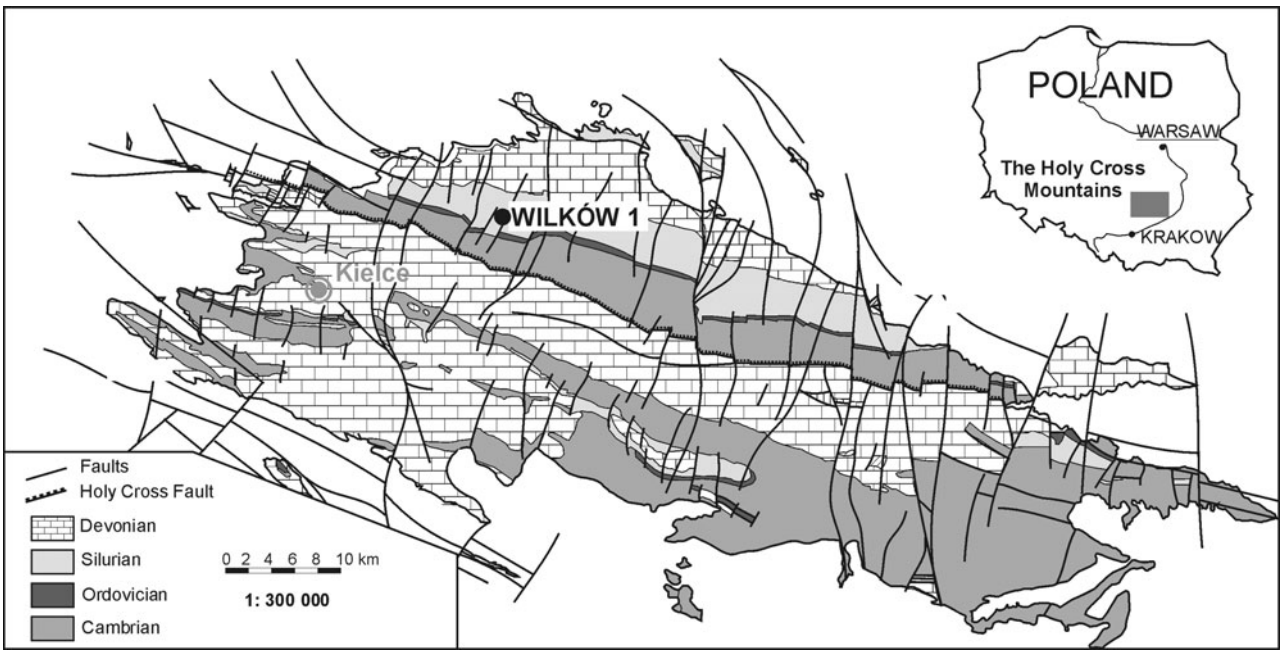

Figure 1. Schematic geological map of the Holy Cross Mountains showing the location of the Wilków 1 borehole (50° 54′ 44.5″ N, 20° 50′ 59.4″ E).

conditions from a scarcely studied deep-shelf setting using geochemical, petrographical and sedimentological methods. Our palaeoenvironmental proxies have never before (pyrite framboids) or only rarely (inorganic indicators) been applied to the Ireviken extinction event (Emsbo *et al*. 2010; Racki *et al*. 2012).

2. Geological setting

The Holy Cross Mountains (HCM) region of central Poland is traditionally subdivided into the Małopolska Massif (MM) in the south and the Łysogóry Unit (LU) in the north, separated by the Holy Cross Fault (Fig. 1). The MM is considered to be a proximal terrane that separated from Baltica but became reattached some time before late Cambrian/Ordovician times. The LU is treated as a part of the passive margin of this palaeocontinent (Dadlez, Kowalczewski & Znosko, 1994). During Silurian time these units are believed to have occupied a position close to the present SW margin of Baltica, which, according to the reconstruction of Torsvik & Rehnström (2001), Hartz & Torsvik (2002) and Cocks & Torsvik (2005), was located close to 30 °S (Cocks, 2002; Nawrocki *et al*. 2007).

The Silurian system in the HCM consists of up to 300 m of Llandovery – lower Ludlow (Rhuddanian to Gorstian stages) shale and mudstone deposits, which are overlain by a ~2000 m thick succession of the upper Ludlow and Pridoli greywacke sandstones, mudstones and carbonates (Kozłowski, 2008). These sediments filled a foredeep basin that extended from the HCM to the present SW margin of Baltica (Poprawa *et al.* 1999; Narkiewicz, 2002) (Fig. 1). The Rhuddanian part of the Silurian shale and mudstone succession is made up of black shales and cherts that accumulated under upwelling conditions (Kremer, 2005) generated by the SE trade winds (Trela & Salwa, 2007). They belong to the Bardo Formation (op. cit.) and contain a graptolite fauna indicative of the *ascensus/acuminatus*, *vesiculosus* and *cyphus* zones (Tomczyka & Tomczykowa, 1976; Podhalańska & Trela, 2007). The overlying Aeronian to Gorstian sediments are represented by grey/green shales and mudstones interrupted by conspicuous black shale intervals of various thicknesses. In the regional lithostratigraphic subdivision these shales and mudstones are given various informal names (Modliński & Szymański, 2001). The graptolite data indicate that black shale horizons reported in the HCM are coeval with prominent sea-level and palaeoceanographic changes documented by Page *et al*. (2007). A relatively thick black shale interval (up to 9 m thick) occurs at the L/W Series boundary and straddles the lower Sheinwoodian *murchisoni–riccartonensis–flexilis* graptolite zones. This stratigraphic interval is correlated with the worldwide IE.

3. Materials and methods

The Wilków 1 borehole spans almost all of the Lower Silurian (excluding the Rhuddanian and most of the Aeronian) and it records deep-shelf facies. Fifty-three samples were collected from the Llandovery and lower Wenlock strata of the Wilków 1 borehole (Fig. 1), which comprises claystones and black shales (see Deczkowski & Tomczyk, 1969). Owing to the relatively high thermal maturation of the sediments (within the 'gas window'; conodont alteration index: CAI > 2, Narkiewicz, 2002; vitrinite-like maceral values calculated to vitrinite reflectance VR_{equ} = ~1.7 %, Smolarek *et al.* 2014), our research has focused on redox proxies

https://doi.org/10.1017/S0016756815001065 Published online by Cambridge University Press

that are not susceptible to alteration by heat, such as pyrite framboid petrography and trace metal concentrations. Sedimentological observations of colour, lithology, sedimentary structures and ichnofabric are supported by thin-section petrography of microfacies.

3.a. Geochemical signature

3.a.1. Total organic carbon (TOC) and total sulphur (TS)

Total carbon (TC), total inorganic carbon (TIC) and total sulphur (TS) contents were measured in 53 samples using an Eltra CS-500 IR-analyser with a TIC module. TC was determined using an infrared cell detector on CO_2 gas, which was evolved by combustion under an oxygen atmosphere. TIC content was derived from reaction with 15 % hydrochloric acid and CO_2 was determined by infrared detector. Total organic carbon (TOC) was calculated as the difference between TC and TIC. Calibration was made by means of the Eltra standards. Analytical precision and accuracy were better than ± 2 % for TC and ± 3 % for TIC.

3.a.2. Trace metals analysis

Thirty-four rock samples from the Wilków 1 borehole were analysed at AcmeLabs, Vancouver, Canada. Samples were chosen based on their position in the section. Major oxides and several minor elements (Ba, Ni, Sr, Zr, Y, Nb, Sc) were measured using inductively coupled plasma atomic emission spectrometry following a lithium borate fusion and dilute acid digestion of a 0.2 g sample pulp. Two separate inductively coupled plasma mass spectrometry analyses of trace elements were performed to optimize determination of a 31-element suite (Ba, Be, Co, Cs, Ga, Hf, Nb, Rb, Sn, Sr, Ta, Th, U, V, W, Zr, Y, La, Ce, Pr, Nd, Sm, Eu, Gd, Tb, Dy, Ho, Er, Tm, Yb, Lu). The reliability of analytical results was monitored by the analysis of international standard reference materials and duplicate analyses of a few samples. Precision and accuracy of the results were better than ± 0.05 % (mostly ± 0.01 %) for the major elements and generally better than ± 1 ppm for the trace elements.

3.a.3. Pyrite framboid analysis

Pyrite framboid analysis has become a widely used petrographic palaeoredox proxy (e.g. Wignall & Newton, 1998; Bond & Wignall, 2010; Wignall *et al.* 2010). It is especially valuable for evaluating thermally altered or weathered outcrop samples because, while the framboids are sometimes pseudomorphed by iron (oxyhydr)oxides, their distinctive size distributions are retained (Lüning *et al.* 2003). Twenty-eight samples in the form of small chips were polished and examined for pyrite framboid populations using a Philips Environmental Scanning Electron Microscope (ESEM) in back-scattered electron (BSE) mode at the University of Silesia (Sosnowiec, Poland). Framboid diameters (in µm) were measured using the ESEM internal measuring device. Where possible, at least 100 framboids were measured per sample. In samples W 582.3 and W 583.8, fewer than 100 framboids were measured (33 and 36 counts, respectively) owing to their scarcity. The minimum, maximum and mean diameters of framboids in each sample, and their standard deviations, were calculated. Framboid size-frequency distributions are depicted in the form of box and whisker plots (see e.g. Wignall & Newton, 1998), and we have generated histograms to better show the size-frequency distribution within a given framboid population.

4. Results

4.a. Stratigraphy

The Silurian of the Wilków 1 borehole includes upper Llandovery to lower Ludlow mudstones and shales (601.0–417.0 m) overlain by upper Ludlow fine-grained greywackes, mudstones and shales (Deczkowski & Tomczyk, 1969). The older part of the succession consists largely of grey to dark grey and subordinate black shales that belong to an informal lithostratigraphic unit, called the Ciekoty Beds (Fig. 2).

Deczkowski & Tomczyk (1969) reported tectonic contact between the Hirnantian sandy mudstones of the Zalesie Formation (*sensu* Trela, 2006) and Silurian (uppermost Aeronian Stage) shales of the *sedgwickii* Zone (Table 1; Fig. 2), suggesting a hiatus of at least 6 million years in the borehole. Deczkowski & Tomczyk (1969) postulated tectonic zones within the Silurian succession, which may have been responsible for the stratigraphic incompleteness of the Wilków section. Nevertheless, the borehole exposes a prominent 9 m thick black shale that spans the lower Wenlock *murchisoni* and *riccartonensis* graptolite zones and extends up to the *flexilis* Zone (Table 1; Fig. 2). The black shales are bound at their base by grey shales of the lower Telychian *turriculatus* to *crenulata* zones (Deczkowski & Tomczyk, 1969), suggesting that the upper Telychian is missing. It cannot be excluded that the 2 m thick black shale / greenish-grey mudstones below the first appearance of *Cyrtograptus murchisoni* (at a depth of 585.0 m) are upper Telychian (Fig. 2). The Wenlock (lower Sheinwoodian *murchisoni–riccartonensis–flexilis* graptolite zones) black shales grade upwards into grey shales extending up to the *leintwardinensis* Zone of the lower Ludfordian Stage (Deczkowski & Tomczyk, 1969) (Table 1; Fig. 2).

4.b. Sedimentary facies: distribution and description

Detailed sedimentological study reveals that the apparently monotonous lower Wenlock black shale interval in the Wilków 1 borehole consists of two distinctive facies, each recording its own depositional conditions. The dominant facies is dark grey to black shales, while the second facies comprises light grey to greenish-grey clayey mudstones. The black shales form four

https://doi.org/10.1017/S0016756815001065 Published online by Cambridge University Press

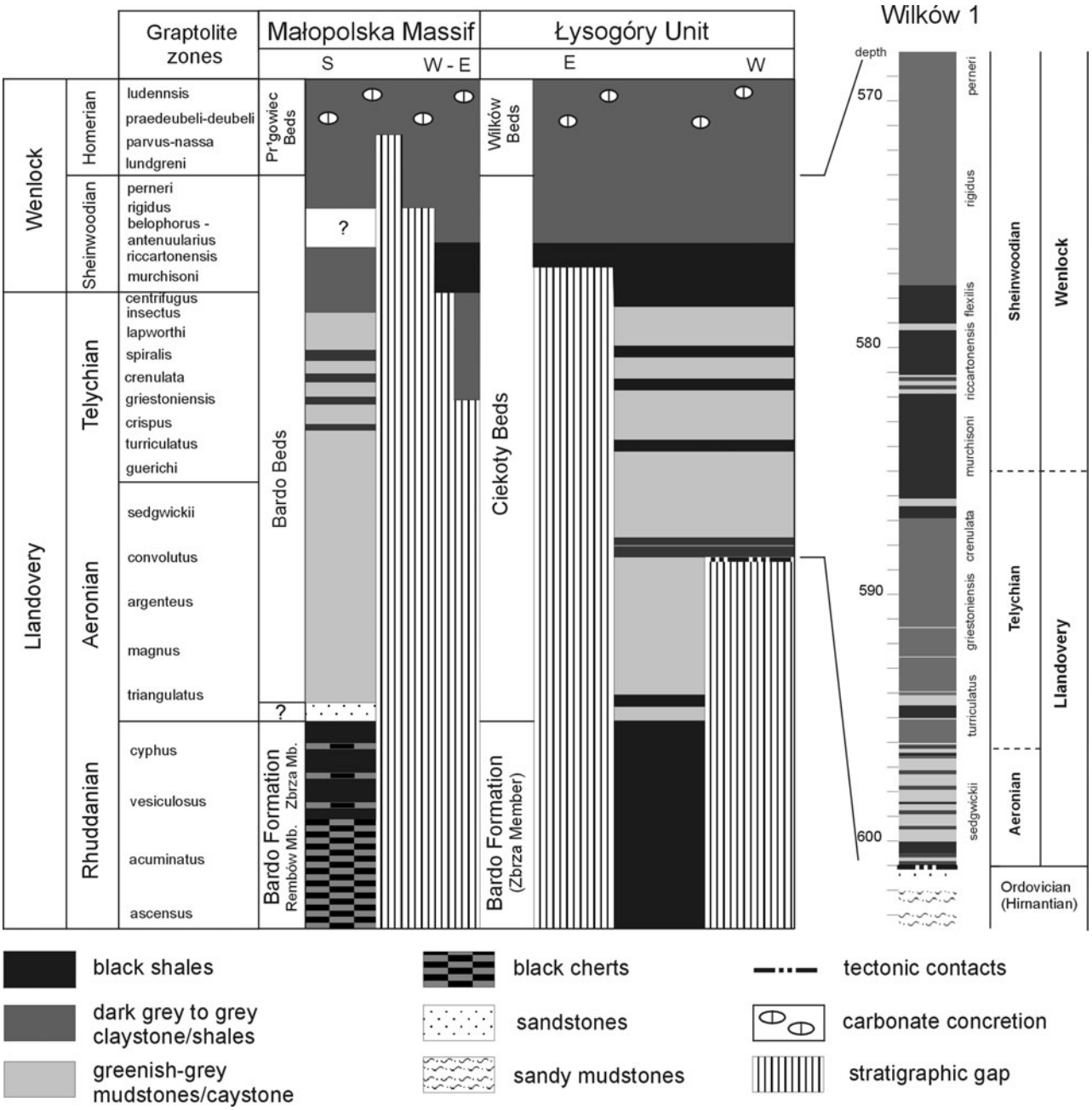

Figure 2. Schematic cross-section showing stratigraphy and facies pattern of the Llandovery and Wenlock in the Holy Cross Mountains (after Malec, 2006, modified) and correlation with the Wilków 1 borehole.

horizons interrupted by thin greenish-grey mudstones that sometimes alternate with thin dark shales (Fig. 2). Graptolite faunas place the lower black shale horizons within the *murchisoni* Zone and the upper black shales within the *riccartonensis–flexilis* zones (Table 1; Fig. 2). The sandwiched greenish-grey mudstone intervals appear to correlate with the uppermost Telychian (or Llandovery/Wenlock boundary), lower *riccartonensis* and lower *flexilis* zones (Table 1; Fig. 2).

The dark grey to black shales reveal conspicuous lamination on a submillimetre to millimetre scale, enhanced by light grey mudstone laminae (Fig. 3a–d). Black laminae are enriched in fine short fibres of organic matter, which in some cases are wrinkled and usually located parallel to the lamina surface (Fig. 3b). The detrital material (silt-size quartz and mica flakes), pyrite framboids and carbonate crystals are trapped between fibres. The mudstone laminae consist of fine silt-sized quartz and are apparently homogeneous; however, some of them show subtle normal grading and discrete mottling as a result of bioturbation (Fig. 3b). Their contact with the black shale laminae is seen to be variously gradational and sharp. This facies exhibits subordinate erosional surfaces (Fig. 3c) and common, tiny mudstone clasts of submillimetre size that appear as light and rounded spots in the darker matrix (Fig. 3c).

The grey and greenish-grey mudstones are present both as thin beds and as intervals of several dozen centimeteres (Fig. 3e). They are largely homogeneous with

https://doi.org/10.1017/S0016756815001065 Published online by Cambridge University Press

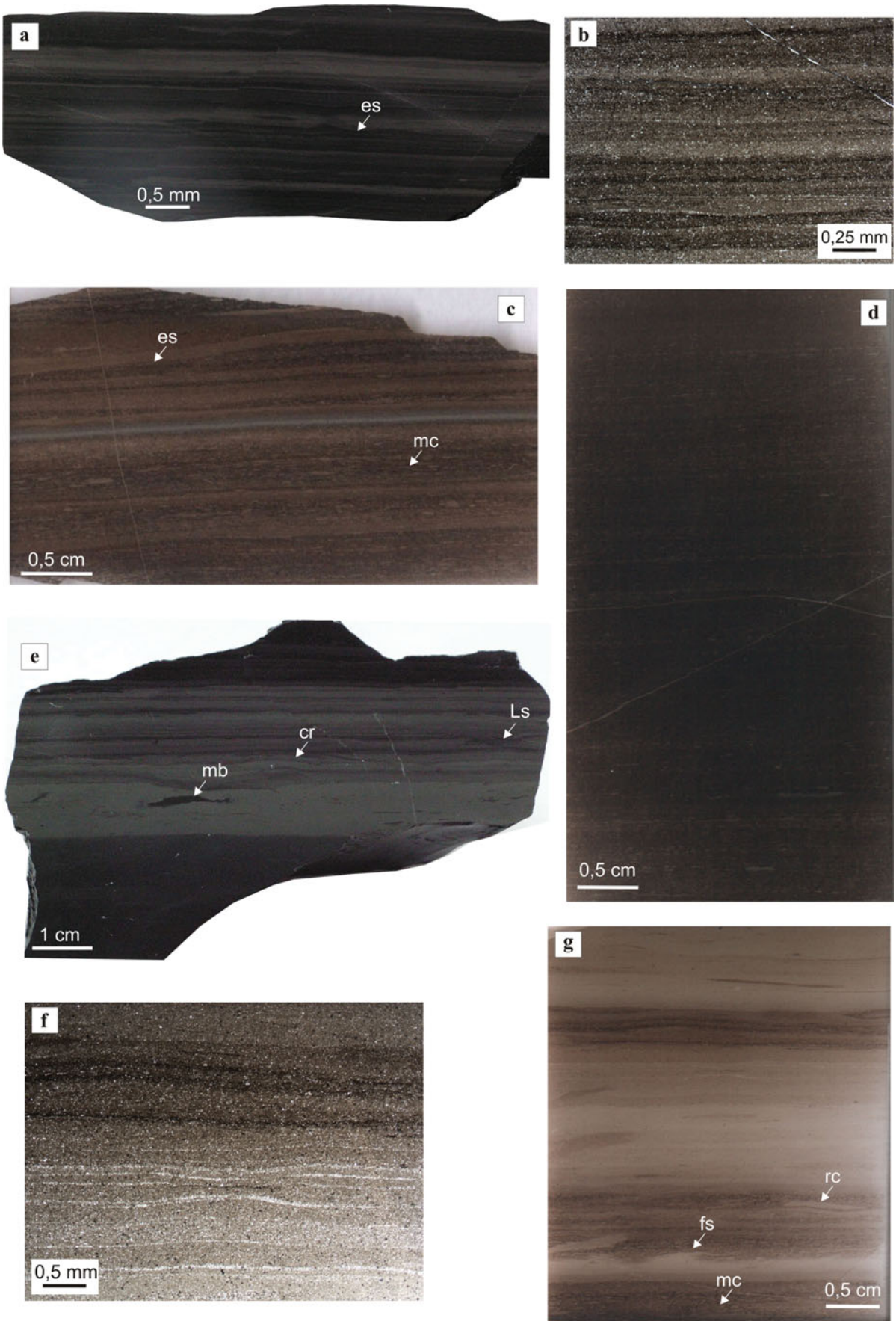

Figure 3. (Colour online) Sedimentological features of the lower Sheinwoodian rocks from the Wilków 1 borehole. (a) Distinct light laminae with subtle normal grading interrupting dark shales. Note discrete mottling bioturbation within light laminae and erosional surface (es) at its base cutting the underlying dark shale. (b) Photomicrograph showing details of (a) (plane polarized light); black laminae enriched in short fibres of organic matter and pyrite framboids intercalated with mudstone laminae. Note scattered

https://doi.org/10.1017/S0016756815001065 Published online by Cambridge University Press

Table 1. Graptolite biozones recognized by Deczkowski & Tomczyk (1969) in grey and black shales

Stratigraphy			Graptolite biozones	Accompanying species
Silurian	Wenlock	Sheinwoodian	*Cyrtograptus rigidus* and *C. perneri* zones	*Monograptus flemingi primus*, *Monoclimacis flumendosae*, *Streptograptus retroflexus*, *Monograptus latus*, *Pristiograptus pseudodubius, Monograptus flemingi*.
			Monograptus antennularius	*M.flexilis*
			Cyrtograptus murchisoni and *Monograptus riccartonensis* zones	*Monograptus priodon*, *Monoclimacis vomerina, Cyrtograptus murchisoni bohemicus*, *Pristiograptus cf. dubius*
	Llandovery	Aeronian to Telychian	*Stimulograptus sedgwickii* to *Monoclimacis crenulata* zones	*Spirograptus* cf. *turriculatus, M.* cf. *griestoniensis*, *Pristiograptus nudus*, *Monograptus marii*, *M. vale*

subordinate subtle bioturbation, although some beds reveal flame structures, rip-up clasts, tiny load-casts, inclined microlamination, current ripples and discrete laminae consisting of silt-sized quartz grains (Fig. 3e, f, g). In some cases, mudstone beds are interrupted by dark laminae consisting of submillimetre-size mudstone clasts (Fig. 3g).

4.c. Bulk geochemical data (TOC, TS, CC)

Despite being lithologically rather similar, the tested samples are characterized by major variations in TOC, ranging from *c*. 0.2 % to 2.7 % (Table 2; Fig. 4). TOC values in the Aeronian and Telychian samples do not usually exceed 0.5 %. TOC content increases just before the Telychian/Sheinwoodian (Llandovery/Wenlock) boundary, and during the Ireviken black shale sedimentation TOC values fluctuate between 0.6 % and 2.7 % (Fig. 4). Younger Sheinwoodian samples are characterized by relatively stable and generally higher TOC values in the range of 1.5 % to 2.2 %. The TS record follows a similar pattern to that of TOC concentration, excluding a single sample (W 583.0) that is very rich in TS but poor in TOC (possibly owing to hydrothermal mineralization by sulphides: see e.g. Rubinowski, 1969). Thus, a good correlation between TOC and TS ($R^2 = 0.7$) is observed, suggesting normal marine deposition (Sageman & Lyons, 2004). Carbonate content (CC) does not exceed 20 % by weight, and in most of the samples ranges between 3 % and 10 %.

4.d. Trace metal palaeoredox proxies

Generally, all of our inorganic redox proxies are in accordance with, and are indicative of, a variety of bottom-water redox conditions (Fig. 5). Only the Ni/Co ratio values are out of step with other data (this is not unusual, see Racka *et al.* 2010), and we have not included Ni/Co in Figure 5. The lack of correlation between the Ni/Co ratio and other trace metal proxies might be attributed to upwelling activity (resulting in Co depletion; Brumsack, 2006), especially in the upper part of the section, and/or very unstable redox conditions at the L/W boundary that led to partial pyrite oxidation and release of Co and Ni (see Tribovillard *et al.* 2006; Swanner *et al.* 2014). The V/(V + Ni), V/Cr and U/Th ratios, and Mo and U concentrations are low through almost the entire Aeronian and Telychian (excluding some elevated values at the beginning of the Aeronian noted for e.g. sample W 601.0). The V/(V + Ni) ratio does not exceed 0.7, U/Th ranges from 0.2 to 0.4, V/Cr ranges from 1 to 2, authigenic uranium (U_{authig}) is below 1 and Mo is about 2 ppm. U/Mo fluctuates between 1.5 and 3.7 (Table 3).

The uppermost Telychian and the IE in the basal Sheinwoodian record an increase in all inorganic redox proxy ratios, as well as Mo concentrations and U_{authig} content (and also a decrease in U/Mo, which subsequently becomes rather unstable). This is consistent with the development of reducing conditions across the Telychian/Sheinwoodian boundary (Fig. 5; Table 3). Following a short phase during which these proxy values decreased, they once again increased and stabilized for the duration of the Sheinwoodian, with values characteristic of anoxic/euxinic conditions (V/(V + Ni) and U/Mo) or of dysoxic (and sporadically oxic) environments (U/Th, U_{authig} and V/Cr) (Table 3). A similar discrepancy whereby V/(V + Ni) exhibits a similar pattern to the other inorganic proxies, but is suggestive of more oxygen-restricted regimes, has been recognized in other basins (Rimmer, 2004; Racka *et al.* 2010).

silt-sized quartz grains forming discrete laminae. (c) Laminated dark shales with light mudstone laminae, erosional surface (es) cutting laminated sediment. Note numerous tiny sub-rounded mudstone clasts (mc) in dark sedimentary background. (d) Wispy and discontinuous mudstone laminae interrupting organic-rich background. (e) Grey/green clayey mudstone interbeds with alternating black shale layers showing mottling bioturbation (mb) in the lower part and parallel lamination in its upper portion, discrete normal grading within the light laminae, current ripples (cr) and load-cast structures (Ls). (f) Photomicrograph showing discontinuous laminae consisting of silt-sized quartz grains within mudstone beds (plane polarized light). Note dark organic and pyrite-rich laminae in the upper part of photomicrograph. (g) Mudstone with flame structure (fs), rip-up clasts (rc) and tiny mudstone clasts (mc) occurring as light and sub-rounded spots in dark sedimentary background.

https://doi.org/10.1017/S0016756815001065 Published online by Cambridge University Press

Table 2. Percentage content of total organic carbon (TOC (%)), carbonate content (CC (%)) and total sulphur (TS (%)) in samples from the Wilków 1 borehole

Sample	TOC [%]	CC [%]	TS [%]	Sample	TOC [%]
W 561.0	1.46	12.32	1.21	**W 581.6**	0.21
W 569.0	1.64	9.75	1.17	**W 582.5**	0.72
W 571.0	1.50	7.87	1.14	**W 583.6**	0.94
W 573.0	1.81	20.09	1.28	**W 584.5**	2.01
W 574.5	1.80	17.62	1.39	**W 585.5**	1.91
W 576.0	2.19	7.91	1.47	**W 586.5**	0.98
W 577.5	2.18	6.35	1.50	**W 587.4**	0.12
W 579.3	2.08	7.15	1.51	**W 588.4**	0.28
W 579.8	2.20	6.72	1.38	**W 589.0**	0.05
W 580.5	1.58	4.09	0.58	**W 589.8**	0.14
W 581.1	2.72	6.40	1.27	**W 590.5**	0.11
W 581.6	1.30	3.47	0.35	**W 591.8**	0.10
W 582.3	0.62	4.34	0.10	**W 592.8**	0.27
W 583.0	2.02	3.24	2.38	**W 593.3**	0.12
W 583.8	1.19	3.54	0.15	**W 594.5**	0.12
W 585.5	1.34	0.90	0.08	**W 595.5**	0.12
W 586.0	0.73	5.22	0.28	**W 596.5**	0.82
W 587.1	0.33	2.94	0.02	**W 597.2**	0.51
W 588.0	0.31	4.40	0.01	**W 598.5**	0.96
W 590.7	0.34	2.58	0.00	**W 599.0**	0.05
W 591.1	0.40	1.15	0.01	**W 599.4**	0.05
W 591.8	0.47	3.91	0.00	**W 600.0**	0.05
W 592.0	0.29	8.13	0.00	**W 600.5**	0.10
W 594.3	0.23	0.17	0.04	**W 601.0**	0.05
W 594.5	0.28	1.56	0.01	**W 602.4**	1.66
W 596.3	0.76	0.45	0.03		
W 596.5	1.39	0.17	1.30		
W 600.9	0.48	0.22	0.22		

4.e. Pyrite framboids

Pyrite framboids are common in almost all the Llandovery and Wenlock shales, excluding Telychian samples between 594.3 and 587.1 m depth, where framboids were absent but euhedral pyrite and other sulphides (e.g. sphalerite) are recorded.

The Rhuddanian and Aeronian samples contain abundant small framboids (mean diameters around 5 μm), with low standard deviations (Table 4). The beginning of the Telychian is marked by the disappearance of framboids, which remained absent through most of the stage. Small framboids reappear at the end of the Telychian, at a depth of 586.0 m in the borehole. The samples from the IE interval are characterized by very rapid fluctuations in pyrite framboid size distributions and in their standard deviations (Table 4; Fig. 4). For example, in the laminated shale at depth 585.0 m, pyrite framboids occur along individual laminae. Analyses of framboids from individual laminae (negating time-averaging effects, see Wignall *et al.* 2010) yield different framboid size frequencies, suggesting rapidly changing conditions (in this case from anoxic/euxinic to upper dysoxic) (Fig. 6a, b). In sample W 598.2 the contact between lighter and darker sediments separates very different framboid populations (in the lighter layer framboids suggest dysoxic conditions, while the darker layer contains a framboid population characteristic of anoxia/euxinia) (Fig. 6c, d). Above the Telychian/Sheinwoodian boundary framboid diameters have a very narrow range (mean *c*. 4.0 μm, SD *c*. 1.0), typical of restricted, oxygen-free conditions.

5. Discussion

5.a. Facies evolution on the basis of the sedimentological record

The lower Wenlock (Sheinwoodian) benthic oxygenation history and associated sea-level changes recorded in the Wilków 1 borehole were likely driven by major early Sheinwoodian climatic changes (compare Page *et al*. 2007). Thus, sedimentological and stratigraphic data from South America indicate that Llandovery and early Wenlock times saw the expansion of glaciation on Gondwana (Díaz-Martínez & Grahn, 2007) driving third-order eustatic sea-level changes and consequently impacting on palaeoceanographic conditions (Loydell, 2007; Lehnert *et al*. 2010). In sequence stratigraphic terms, black shales record either the basal part of the transgressive systems tract or the maximum flooding surface (Wignall, 1991; Wignall & Maynard, 1993). In the lower Sheinwoodian shale and mudstone succession of the LU, the black shales derived from sediment starvation and oxygen-deficient conditions during deglacial transgressive periods that favoured the development of benthic microbial mats and biofilms that are preserved as organic matter fibres. However, the fine silt material in the lighter coloured laminae indicate periodic deposition from diluted low-density bottom currents, or dust clouds of aeolian origin interrupting accumulation of hemipelagic organic-rich clays (see O'Brien, 1996). Tiny mudstone micro-clasts within the dark laminae probably originated from the intermittent erosion of a partially consolidated mudstone substrate and subsequent transport by bottom currents (see

https://doi.org/10.1017/S0016756815001065 Published online by Cambridge University Press

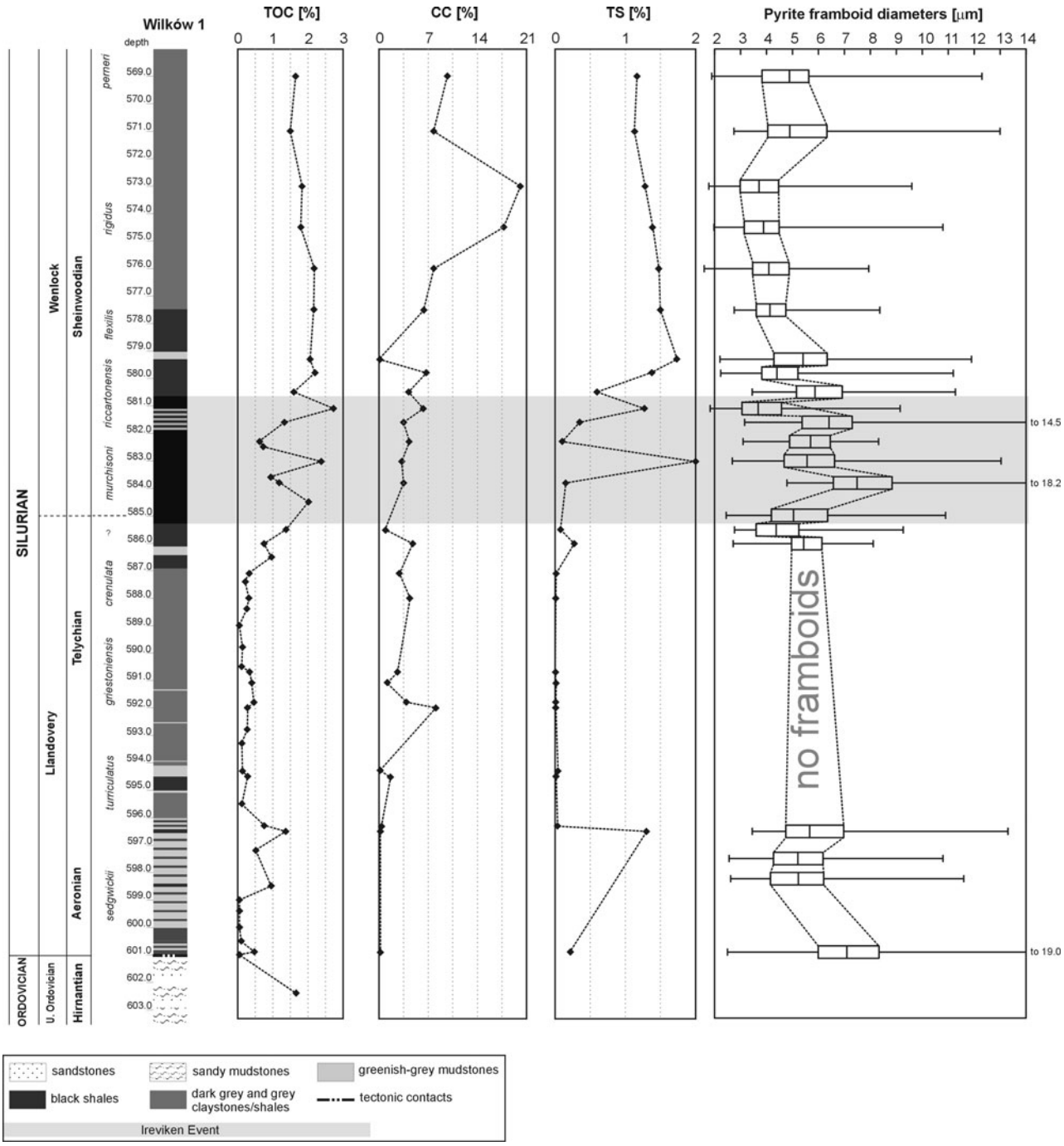

Figure 4. Composite plot of the Wilków 1 borehole showing total organic carbon content (TOC (%)), carbonate content (CC (%)), total sulphur (TS (%)) and pyrite framboid diameters (μm) (see Table 2).

Schieber, Southard & Schimmelmann, 2010). A similar fabric has been interpreted elsewhere as the result of accumulation of faecal pellets or burrow fills modified by compaction (op. cit.). The activity of bottom currents contributed to short-lived oxygenation events in the LU sedimentary basin and to periodic water-column mixing (compare with Schieber, 1994).

The Sheinwoodian greenish-grey mudstones record periods of benthic oxygenation that promoted bioturbation and subsequent homogenization of the muddy sediment. The occurrence of discrete erosional (rip-up clasts, cut and fill, and flame structures) and sedimentary structures within this facies suggest that bottom currents influenced sedimentary conditions. According to Page *et al*. (2007) this type of shale and mudstone facies can result from water-column ventilation in response to increased thermohaline circulation during the glacial maxima and regressions.

Graptolite faunas clearly correlate the lower Wenlock black shale horizons in the LU with the *murchisoni* and late *riccartonensis* Zone sea-level highs postulated by Loydell (1998) and Loydell & Frýda (2007). The black shales are interrupted by a relatively short interval of increased greenish-grey mudstone intercalations, which may reflect sea-level fall from the late *murchisoni* to early *riccartonensis* graptolite zones (op. cit.).

https://doi.org/10.1017/S0016756815001065 Published online by Cambridge University Press

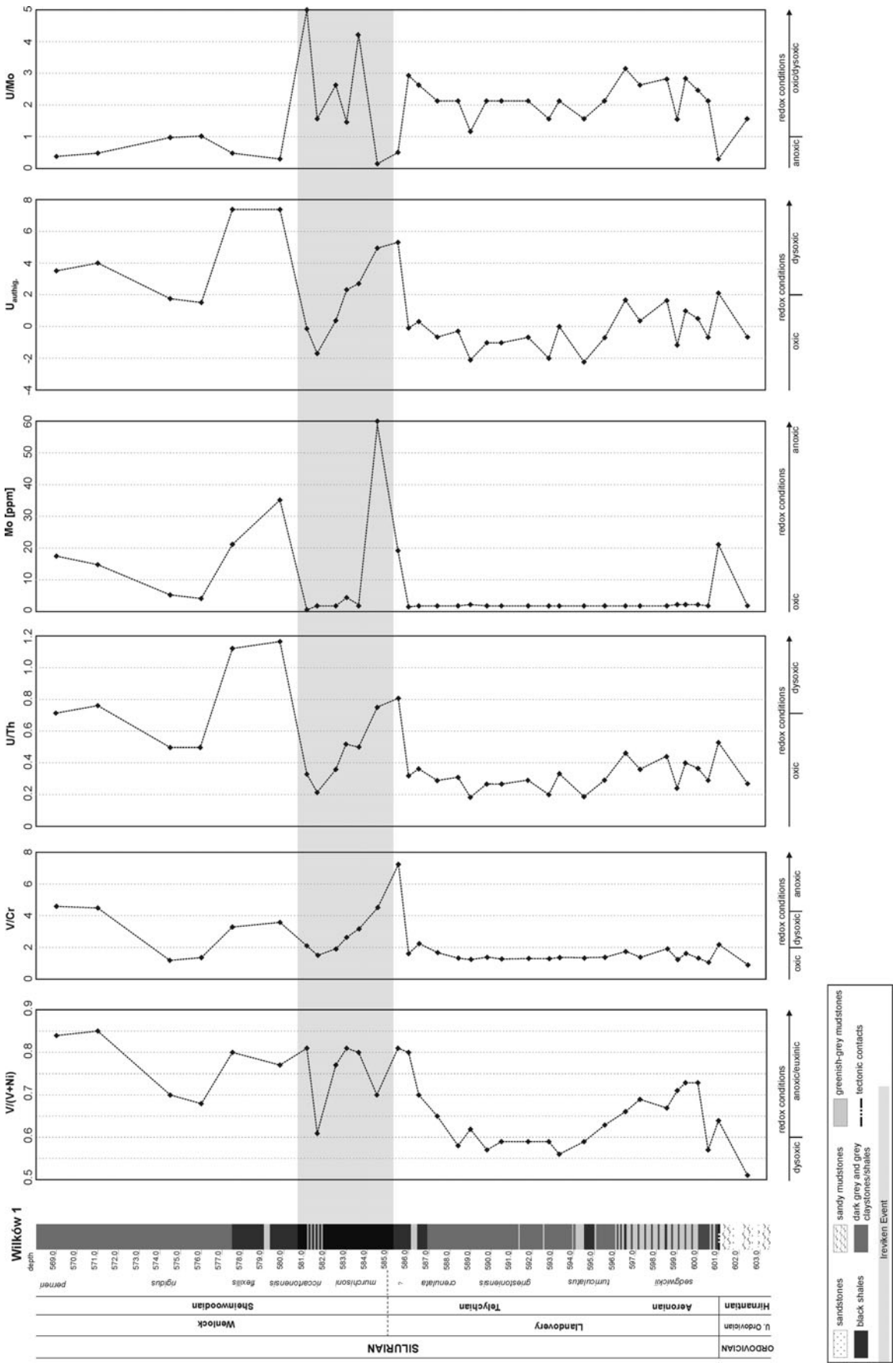

Figure 5. Stratigraphic distribution of the trace metal redox indicators across the Wilków 1 borehole (see Table 3).

https://doi.org/10.1017/S0016756815001065 Published online by Cambridge University Press

Table 3. Evolving palaeoredox conditions interpreted for the Wilków 1 borehole as indicated by different trace metals ratios

Sample	V ppm	Ni ppm	Cr ppm	U ppm	Th ppm	Mo ppm	$U_{authig.}$ #	U/Mo	V/(V+Ni)	V/Cr	U/Th
W 561.0	199.0	71.6	82.1	7.6	10.0	17.2	4.3†	0.44	0.74‡	2.42†	0.76†
W 569.0	380.0	71.3	82.1	6.5	9.1	17.0	3.5†	0.38	0.84§	4.63‡	0.71*
W 571.0	402.0	69.2	88.9	7.2	9.5	14.7	4.0†	0.49	0.85§	4.52‡	0.76†
W 574.5	94.0	39.4	75.3	5.0	10.0	5.1	1.7*	0.98	0.70‡	1.25*	0.50*
W 576.0	97.0	45.7	68.4	4.5	9.0	4.4	1.5*	1.02	0.68‡	1.42*	0.50*
W 577.5	300.0	75.1	88.9	10.5	9.3	21.3	7.4†	0.49	0.80‡	3.37†	1.13†
W 579.8	298.0	89.4	82.1	10.4	8.9	35.4	7.4†	0.29	0.77‡	3.63†	1.17†
W 581.1	227.0	52.1	109.5	4.5	13.7	0.9	− 0.1*	5.00	0.81‡	2.07†	0.33*
W 581.6	99.0	63.0	66.0	3.0	14.0	1.9	− 1.7*	1.58	0.61‡	1.50*	0.21*
W 582.5	130.0	38.0	68.0	5.0	14.0	1.9	0.3*	2.63	0.77‡	1.91*	0.36*
W 583.0	251.0	57.4	95.8	6.6	12.8	4.5	2.3†	1.47	0.81‡	2.62†	0.52*
W 583.6	165.0	42.0	52.0	8.0	16.0	1.9	2.7†	4.21	0.80‡	3.17†	0.50*
W 584.5	249.0	105.0	55.0	9.0	12.0	60.0	5.0†	0.15	0.70‡	4.53‡	0.75†
W 585.5	332.0	77.0	46.0	9.0	11.0	18.0	5.3†	0.50	0.81‡	7.22‡	0.82†
W 586.0	151.0	37.3	95.8	4.4	13.6	1.5	− 0.1*	2.93	0.80‡	1.58*	0.32*
W 586.5	143.0	61.0	65.0	5.0	14.0	1.9	0.3*	2.63	0.70‡	2.20†	0.36*
W 587.4	105.0	57.0	63.0	4.0	14.0	1.9	− 0.7*	2.11	0.65‡	1.67*	0.29*
W 588.4	92.0	68.0	69.0	4.0	13.0	1.9	− 0.3*	2.11	0.58†	1.33*	0.31*
W 589.0	99.0	60.0	80.0	2.4	13.4	2.0	− 2.1*	1.18	0.62‡	1.24*	0.18*
W 589.8	99.0	75.0	71.0	4.0	15.0	1.9	− 1.0*	2.11	0.57†	1.39*	0.27*
W 590.5	96.0	66.0	76.0	4.0	15.0	1.9	− 1.0*	2.11	0.59†	1.26*	0.27*
W 591.8	89.0	63.0	67.0	4.0	14.0	1.9	− 0.7*	2.11	0.59†	1.33*	0.29*
W 592.8	96.0	68.0	76.0	3.0	15.0	1.9	− 2.0*	1.58	0.59†	1.26*	0.20*
W 593.3	79.0	62.0	58.0	4.0	12.0	1.9	0.0*	2.11	0.56†	1.36*	0.33*
W 594.5	95.0	67.0	72.0	3.0	16.0	1.9	− 2.3*	1.58	0.59†	1.32*	0.19*
W 595.5	113.0	65.0	84.0	4.0	14.0	1.9	− 0.7*	2.11	0.63‡	1.35*	0.29*
W 596.5	157.0	80.0	91.0	6.0	13.0	1.9	1.7*	3.16	0.66‡	1.73*	0.46*
W 597.2	140.0	64.0	97.0	5.0	14.0	1.9	0.3*	2.63	0.69‡	1.44*	0.36*
W 598.5	180.0	89.0	94.0	7.0	16.0	1.9	1.7*	3.68	0.67‡	1.91*	0.44*
W 599.0	123.0	50.0	100.0	3.1	13.0	2.0	− 1.2*	1.57	0.71‡	1.23*	0.24*
W 599.4	164.0	60.0	100.0	5.7	14.1	2.0	1.0*	2.84	0.73‡	1.64*	0.40*
W 600.0	135.0	50.0	100.0	4.9	13.2	2.0	0.5*	2.46	0.73‡	1.35*	0.37*
W 600.5	101.0	77.0	95.0	4.0	14.0	1.9	− 0.7*	2.11	0.57†	1.06*	0.29*
W 601.0	196.0	110.0	90.0	6.0	11.6	21.0	2.1†	0.29	0.64‡	2.18†	0.52*
W 602.4	86.0	82.0	93.0	3.0	11.0	1.9	− 0.7*	1.58	0.51†	0.92*	0.27*

 # $U_{authig.} = U_{total} - Th_{total}/3$

Bottom-water redox conditions

	$U_{authig.}$	V/(V+Ni)	V/Cr	U/Th
Oxic*	< 2	< 0.46	< 2	< 0.75
Dysoxic†	2.0–10.0	0.46–0.60	2.00–4.25	0.75–1.25
Anoxic‡	10.0–15.0	0.54–0.82	> 4.25	> 1.25
Euxinic§	> 15.0	≥ 0.84–0.89		
Source of data	*(3)*	*(1)*	*(2)*	*(2)*

Threshold values: (1) Hatch & Leventhal (1992); (2) Jones & Manning (1994); (3) Wignall (1994).

Thin green mudstones above the upper *riccartonensis* black shales appear to be coeval with Loydell's (1998) short-term regressive–transgressive event during the *flexilis* Zone (Table 1). As is the case in the eastern Baltic area (Loydell, 1998; Kaljo & Martma, 2006), there is a stratigraphic gap in the Wilków section that spans the upper Telychian and appears to be related to sea-level fall during this time interval. The base of the considered black shale interval may be of uppermost Telychian age, but a lack of precise biostratigraphic data hampers any sequence stratigraphic correlations and sea-level reconstructions.

5.b. Reconstruction of depositional environments based on integrated geochemical proxies

There is general correspondence between TOC and our inorganic redox proxies, which reveal repeated changes in benthic oxygenation. Two peaks in TOC occur near the Aeronian/Telychian boundary and during the lower Telychian. The later phase of enhanced TOC continued across the Telychian/Sheinwoodian boundary and (with some fluctuations) well into the Sheinwoodian (Figs 4, 5). The TOC increase associated with the Aeronian/Telychian boundary is probably the local manifestation of the so called 'Sandvika event' (Calner, 2008), but there is lack of comparable data from other worldwide sections. Similar TOC values from the Sheinwoodian (basal Wenlock) were reported by Loydell & Frýda, (2007) from the Banwy River section, Wales, and by Racki *et al*. (2012) from Podolia, Ukraine, and patterns are similar to those presented here. In both cases authors reported a noticeable increase in TOC concentration in the lower Wenlock deposits, but in those relatively shallow facies absolute values are two to three times lower than those observed in the HCM. Vandenbroucke *et al*. (2013) inferred that

https://doi.org/10.1017/S0016756815001065 Published online by Cambridge University Press

Table 4. Pyrite framboid data from Wilków 1 borehole

Sample	Min FD [μm]	Max FD [μm]	Mean [μm]	SD	N
W 561.0	1.8	9.4	4.72	1.26	100
W 569.0	1.9	12.3	4.95	1.64	100
W 571.0	2.8	13.0	5.39	1.83	100
W 573.0	1.8	9.6	3.92	1.37	100
W 574.5	2.0	10.8	4.08	1.34	100
W 576.0	1.6	7.9	4.21	1.23	100
W 577.5	2.4	8.2	3.93	0.99	100
W 579.3	2.2	11.9	5.37	1.52	100
W 579.8	2.2	11.2	4.65	1.38	100
W 580.5	3.1	11.2	5.81	1.38	100
W 581.1	1.8	9.2	3.91	1.25	100
W 581.6	3.2	14.5	6.74	2.20	100
W 582.3	3.1	8.3	5.62	1.18	33
W 583.0	2.3	13.0	5.53	1.90	100
W 583.8	4.8	18.2	8.17	2.72	36
W 585.0	2.5	10.9	5.35	1.69	100
W 585.5	2.8	9.3	4.55	1.19	100
W 586.0	2.3	7.9	5.19	1.04	100
W 596.5	3.5	13.3	6.09	1.91	100
W 597.5	2.6	10.8	5.42	1.60	100
W 598.2	2.6	11.6	5.40	1.57	100
W 600.9	2.5	19.0	7.24	2.19	100

N – number in sample; SD – standard deviation; FD – framboid diameter.

primary productivity increased just before the IE on the basis of sections in Gotland. Further afield, Noble *et al*. (2005) noted a sharp increase in TOC to 3 % precisely at the Telychian/Sheinwoodian boundary in the deep-water Cape Phillips Formation, Arctic Canada, followed by a similarly sharp decrease to < 1 % during the *centrifugus–insectus* Zone (Table 1). The above data suggest that in deeper shelf settings TOC enrichment began prior to the L/W boundary while in shallow-water sections this did not begin until after L/W boundary. This implies that oxygen-depleted waters expanded from the deeper parts of the basin (compare to the model of Hammarlund *et al*. 2012 proposed for the Ordovician/Silurian boundary) and reached the deep shelf during early Wenlock time.

Such a scenario is confirmed by our inorganic proxies. U/Th ratios suggest that during the IE, bottom-water conditions changed from being initially oxic at the end of Telychian time to suboxic/anoxic, before returning to oxic for a short time at the end of the event (Fig. 5). A similar history can be inferred from V/Cr values, U_{authig} and Mo concentrations (Table 3). The values of V/(V + Ni) are suggestive of more oxygen-restricted conditions, from dysoxic/anoxic (0.5–0.8, see Table 3) in the basal and middle parts of the section to euxinic (> 0.84) by the upper Sheinwoodian (Fig. 5). We observe general similarities between patterns in the abovementioned redox proxies with the U/Mo ratio, defined recently by Zhou *et al*. (2012) as a depositional environment indicator that distinguishes anoxic/euxinic from dysoxic conditions (Table 3). The U/Mo proxy (Zhou *et al*. 2012) as applied to the Wilków 1 section reveals U/Mo > 1 in the Aeronian and Telychian, suggesting oxygenated conditions. Fluctuating values during the IE include those of < 1 in the Sheinwoodian that are characteristic of an anoxic/euxinic redox environment (Zhou *et al*. 2012).

Elevated TOC near the Aeronian/Telychian boundary, together with increased U/Th and V/(V + Ni) ratios (Fig. 5) and the occurrence of small pyrite framboids (see Section 5.c below), suggests that more oxygen-restricted conditions prevailed during the lesser known Sandvika event. However, other inorganic proxies show no significant changes.

Based on these results, Aeronian sedimentation records dysoxic to anoxic/euxinic conditions, and almost the entire Telychian was oxic. The L/W boundary interval was distinguished by rapidly changing conditions from dysoxic to anoxic/euxinic, even down to the millimetre scale within the studied sediments (Fig. 6). The youngest investigated sediments of the Sheinwoodian Stage yield relatively stable values for all inorganic proxies, indicative of dysoxic to anoxic sedimentary conditions.

5.c. Correlation of pyrite framboid and inorganic redox proxies

Pyrite framboid analysis is routinely used as a palaeoredox proxy and has been applied to marine basins dating back to Ediacaran time (e.g. Wignall & Newton, 1998; Zhou & Jiang, 2009; Bond & Wignall, 2010; Wignall *et al.* 2010; Algeo *et al.* 2011; Hammarlund *et al.* 2012; Marynowski *et al.* 2012; Wang, Shi & Jiang, 2012). Framboids form in waters that are supersaturated with respect to both Fe monosulphides and pyrite in which reaction kinetics favour the formation of the framboidal varieties of the former (Wilkin, Barnes & Brantley, 1996). In euxinic basins the locus of framboid and euhedral pyrite formation is separated by the thickness of the sulphidic water column and often Fe limitation within the sediments ensures that sediments have very high proportions of syngenetic framboids (e.g. Ross & Degens, 1974; Wilkin &

https://doi.org/10.1017/S0016756815001065 Published online by Cambridge University Press

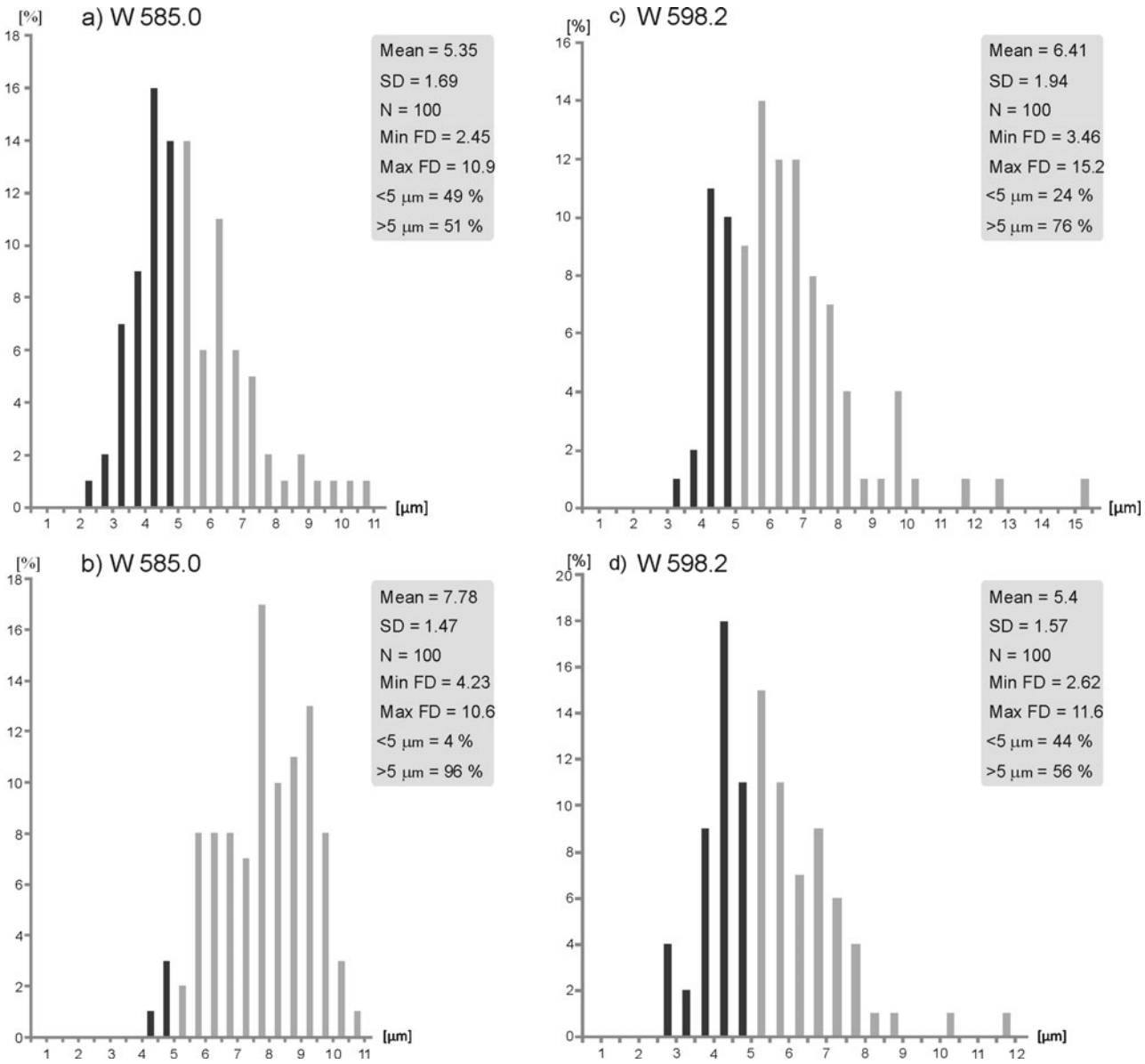

Figure 6. Histograms showing the distribution of pyrite framboids within two adjacent layers in sample W 585.0 (a, b) and two layers in sample W 598.2 (c, light coloured layer; and d, dark coloured layer). Black bars – framboid diameters below 5 µm; grey bars – framboid diameters above 5 µm; mean – mean diameter; SD – standard deviation; N – number of measurements; FD – framboid diameter.

Arthur, 2001). Syngenetic framboids, such as those in the modern Black Sea, rarely reach 6–7 µm diameter before the dense particles sink to the sea bed and accumulate as small-sized populations with a narrow size distribution (Wilkin, Barnes & Brantley, 1996). This resulting size-frequency distribution is useful for identifying ancient euxinia because it contrasts with framboid populations from more oxygenated settings (Wilkin, Barnes & Brantley, 1996; Wilkin & Arthur, 2001). Thus, in dysoxic settings (bottom-water oxygen levels between 0.2 and 2.0 ml O_2/l H_2O), framboids form within the sediment as populations with a broader size distribution and consequently have a larger standard deviation (Wilkin, Barnes & Brantley, 1996). In dysoxic sediments formed in the oxygen-minimum zones offshore of Oman and Angola, framboid populations range up to 20 µm diameter (Schallreuter, 1984; Lallier-Verges, Bertrand & Desprairies, 1993). Shallower-water dysoxic sediments, such as those encountered in Baltic lagoons have similar-sized populations (Neumann *et al.* 2005) as do those of the Mississippi shelf where framboids average 9–13 µm diameter, with a total size range of 4–20 µm diameter (Brunner *et al.* 2006).

Pyrite populations of euxinic and dysoxic settings are clearly distinguishable; however, the distinction between euxinic and suboxic sediments (forming in bottom waters of 0.0–0.2 ml O_2/l H_2O) is less clear cut. Recent suboxic sediments from the Santa Barbara Basin have very small framboid populations at some levels that are typical of those encountered in euxinic basins (Schieber & Schimmelmann, 2006, 2007). It

https://doi.org/10.1017/S0016756815001065 Published online by Cambridge University Press

may be that the smaller framboid populations settled from the water column during transient euxinia – brief phases that would be impossible to distinguish in the geological record, owing to the time-averaging effect of analysing a rock chip typically of 1–2 cm thickness. This effect is particularly notable in environments subject to high-amplitude redox changes. The Salton Sea, a hypereutrophic lake in southern California, experiences summer euxinia and winter oxia. Its sediments contain abundant framboids showing a narrow size-frequency distribution around 5 μm that record the euxinic phases (De Koff, Anderson & Amrhein, 2008) but not the oxic phases. However, redox fluctuations in the HCM are likely to have been less dynamic at the yearly-to-decadal scale owing to the large water masses involved.

Comparing TOC and inorganic palaeoredox indicators with pyrite framboid size distributions in the Wilków 1 borehole (Figs 4, 5) yields a good correlation between all (in particular there is strong agreement in redox inferred from pyrite framboids and the V/(V + Ni) ratio). Pyrite framboids are absent from almost all of the Llandovery section (10 m thick), which also records very low TOC and low inorganic proxy values. During the Telychian/Sheinwoodian boundary interval, all proxies display sharp fluctuations (on the centimetre scale) that indicate a full range of conditions from oxic/dysoxic to euxinic. Above the 6 m thick Telychian/Sheinwoodian boundary interval, most of our redox proxies stabilized. Thus, Wenlock sedimentary rocks contain exclusively small pyrite framboid diameters and relatively high concentrations of redox-sensitive trace metals, typical of anoxic/euxinic conditions.

5.d. Causes and consequences of sea-level changes

Three major episodes of L/W boundary sedimentation can be reconstructed, based on new data:

(i) Pre-IE times (Telychian Stage) record a sea-level lowstand, intensive water circulation and low productivity. Such conditions might have resulted from sea-level fall (Ross & Ross, 1996; Brett *et al*. 2009 but see also Loydell, 1998; Johnson, 2006, 2010; Spengler & Read, 2010; review in: Munnecke *et al*. 2010; Melchin, Sadler & Cramer, 2012) that may be connected with icehouse pulses (Page *et al*. 2007).

(ii) During the IE the basin saw intensive chemocline fluctuations during a marine transgression and moderate productivity. The late Telychian sea-level rise and transgression was probably associated with deglaciation, during which sedimentary conditions on the deep shelf became oxygen restricted. Very intense anoxic/euxinic zone oscillations are recorded by both inorganic proxies and pyrite framboids (Figs 4, 5). Typically, rapid chemocline fluctuations result in time-averaged geochemical and petrographic redox proxies that might be interpreted as a signal of dysoxia, but might actually derive from short-lived, repeated oxic to anoxic–euxinic transitions. Rapid fluctuations of the chemocline in the water column, reported also by McLaughlin, Emsbo & Brett (2012) represent a potent kill mechanism in the Ireviken mass extinction scenario. Redox changes in the deeper water masses would likely preferentially affect pelagic and hemipelagic organisms (e.g. Jeppsson, 1990; Munnecke, Samtleben & Bickert, 2003). These observations are compatible with reconstructions of depositional conditions based on sedimentological data and stable isotope records through the Ireviken black shale deposition by Page *et al*. (2007) and McLaughlin, Emsbo & Brett (2012). The one discrepancy in each of those studies is the interpretation of the transgression/regression pulse, which stems from the use of different sea-level curves (Ross & Ross, 1996; Johnson, 2010) that record local conditions (see e.g. Brett *et al*. 2009).

Two phases of deposition in our environmental model (Fig. 7a, b) generally correspond to humid (H) and arid (A) periods described by Bickert *et al*. (1997). During A conditions at low latitudes, better ventilated episodes frequently occurred owing to evaporation and downwelling of warm, saline and well-oxygenated surface water. During H periods anoxic deep waters invade deep-shelf areas owing to estuarine water circulation, leading to deposition of black shales. However, Page *et al*. (2007) presented a different interpretation of Silurian sea-level fluctuations closely connected with glacial events, which correlate well with our geochemical results. A third model (Fig. 7c) is proposed for intervals during which inorganic proxies suggest oxic to dysoxic bottom-water conditions, but the predominance of tiny pyrite framboids is typical for the occurrence of a euxinic water column (e.g. Bond & Wignall, 2008). Our data confirm the occurrence of euxinia in the Silurian ocean (see Munnecke, Samtleben & Bickert, 2003), but the application of multiple proxies adds to the possible water-column structure before and during the IE.

(iii) Following the IE, stable conditions developed with a euxinic zone in the water column and dysoxic to sporadically anoxic bottom water and moderate productivity (Fig. 7).

Following the Ireviken black shale sedimentation, redox conditions became more stable for a time, reflected in all of our redox proxies (Figs 4, 5). An anoxic/euxinic zone occurred in the water column (very small pyrite framboids) while the seafloor experienced oxygen-deficient conditions interspersed with episodes of anoxia/euxinia (inorganic redox proxies; Tables 3, 4; Fig. 7).

5.e. Comparison of the model with other Palaeozoic events

A very similar redox history to that presented here for the IE has been described by Hammarlund *et al*. (2012) and Harper, Hammarlund & Rasmussen (2014) for the end-Ordovician mass extinction event (see also Armstrong & Harper, 2014). Similarities between the end-Ordovician and IE have been postulated by Noble

https://doi.org/10.1017/S0016756815001065 Published online by Cambridge University Press

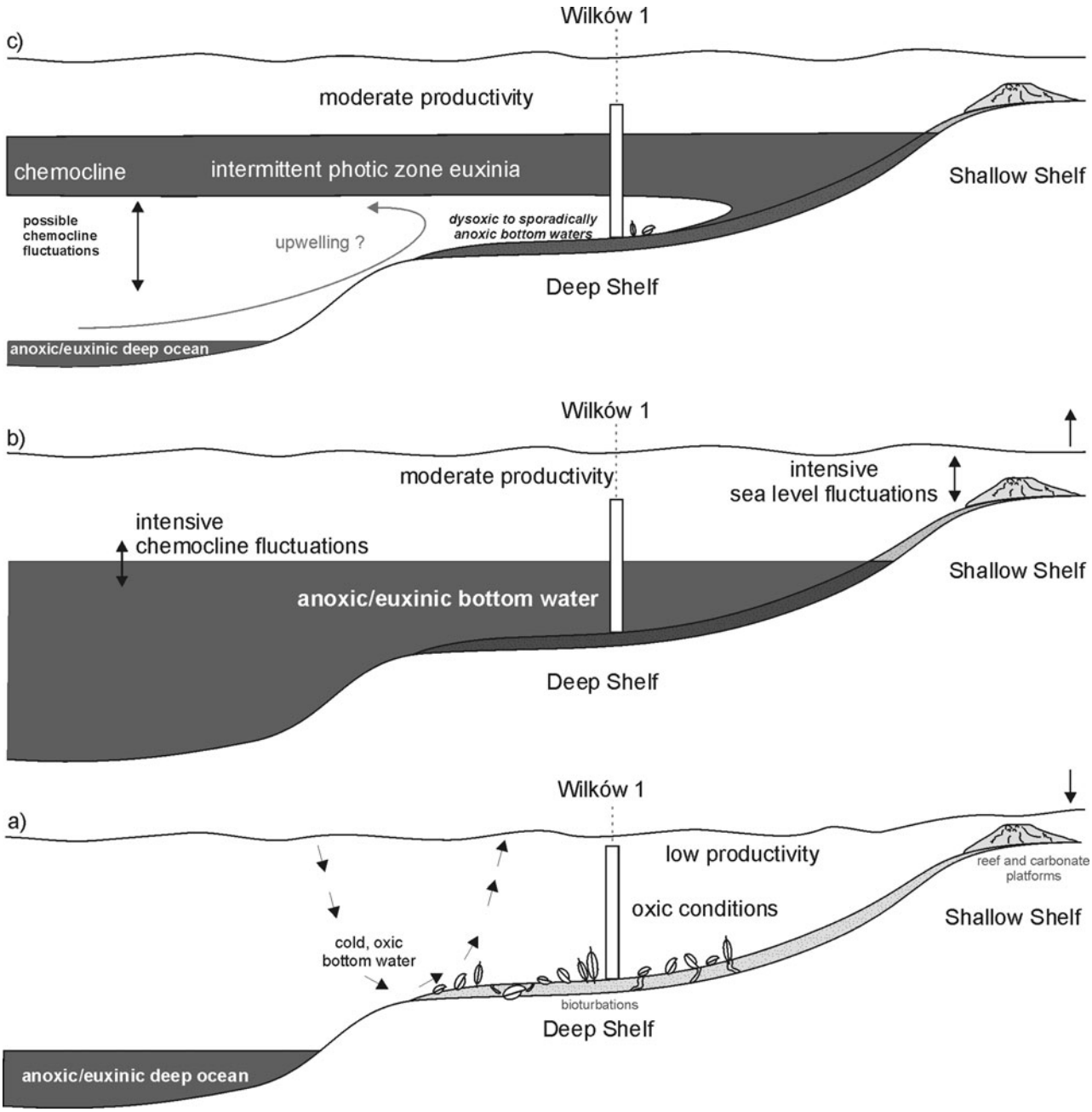

Figure 7. Three conceptual models showing sedimentary conditions detected before, during and after the Ireviken Event: (a) before: oxic to sporadically dysoxic sedimentary conditions during a lowstand, with intensive water circulation and low productivity; (b) during: very intensive chemocline fluctuations caused by transgressive seas with moderate productivity; (c) after: relatively stable conditions with a euxinic zone in the water column and dysoxic to sporadically anoxic bottom waters and moderate productivity.

et al. (2005 and references therein) because of the coincidence of a positive $\delta^{13}C$ excursion, biotic extinction, widespread eustatic low stands and sedimentary hiatuses in shallow waters, sediments that are poor in organic carbon, and the short duration of events. Our data support the assertion that the sedimentary redox record for the Ireviken black shale is analogous to that described from the end-Ordovician event.

In parallel scenarios, fluctuating photic zone euxinia in the water column has been proposed for the much better-known Permian–Triassic Panthalassic Ocean successions (Algeo *et al*. 2011) and Famennian (Upper Devonian) black shales (Marynowski *et al*. 2011, 2012). In both scenarios bottom-water conditions were at least periodically oxic/dysoxic during black shale deposition despite evidence for euxinia in the water column. In the case of Devonian black shales, the existence of a euxinic water column was confirmed by pyrite framboids and biomarkers from green sulphur bacteria (Marynowski *et al.* 2011, 2012; Racka *et al.* 2010). Such palaeoenvironmental scenarios took place with some frequency during Phanerozoic time.

https://doi.org/10.1017/S0016756815001065 Published online by Cambridge University Press

6. Conclusions

(1) Inorganic trace metal redox proxies suggest that during the Ireviken bio-crisis, bottom-water conditions ranged from oxic (Telychian) to mostly suboxic/anoxic (the first phase of the IE) and back to oxic again (the last phase of the IE). Oxygen-depleted waters expanded from the deeper parts of the basin and reached the deep shelf during the first phase of Ireviken black shale deposition. Post-IE conditions stabilized and became anoxic/suboxic on the seafloor with a euxinic zone in the water column.

(2) General similarities are observed in the patterns of all our redox proxies and in the U/Mo ratio. Large variations in these values during Ireviken black shale sedimentation are suggestive of rapid redox fluctuations. Such fluctuations can be connected with deglaciation, in a similar scenario as has been proposed for the Ordovician/Silurian extinction event.

(3) Rapid fluctuations of the chemocline in the water column during the IE were likely a major trigger of the Ireviken mass extinction, which affected mainly pelagic and hemipelagic organisms. Shallow-water dwellers, such as reef ecosystems, were relatively unaffected during the IE.

Acknowledgements. This work was supported by the National Science Center of Poland, grants: 2012/07/B/ST10/04211 (to WT) and 2014/13/N/ST10/03006 (to JS). DB acknowledges his support from the Natural Environment Research Council (Grant NE/J01799X/1). The research was also supported by Wroclaw Research Centre EIT+ within the project 'The Application of Nanotechnology in Advanced Materials' – NanoMat (POIG.01.01.02-02-002/08) financed by the European Regional Development Fund (Innovative Economy Operational Programme, 1.1.2).

References

ALGEO, T. J., KUWAHARA, K., SANO, H., BATES, S., LYONS, T., ELSWICK, E., HINNOV, L., ELLWOOD, B., MOSER, J. & MAYNARD, J. B. 2011. Spatial variation in sediment fluxes, redox conditions, and productivity in the Permian–Triassic Panthalassic Ocean. *Palaeogeography, Palaeoclimatology, Palaeoecology* **308**, 65–83.

ARMSTRONG, H. A. & HARPER, D. A. T. 2014. An earth system approach to understanding the end-Ordovician (Hirnantian) mass extinction. In *Volcanism, Impacts, and Mass Extinctions: Causes and Effects*. pp. 287–300. Boulder, Colorado: Geological Society of America, Special Papers 505.

BICKERT, T., PÄTZOLD, J., SAMTLEBEN, C. & MUNNECKE, A. 1997. Paleoenvironmental changes in the Silurian indicated by stable isotopes in brachiopod shells from Gotland, Sweden. *Geochimica et Cosmochimica Acta* **61**, 2717–30.

BOND, D. P. G. & WIGNALL, P. B. 2008. The role of sea-level change and marine anoxia in the Frasnian–Famennian (Late Devonian) mass extinction. *Palaeogeography, Palaeoclimatology, Palaeoecology* **263**, 107–18.

BOND, D. P. G. & WIGNALL, P. B. 2010, Pyrite framboid study of marine Permian–Triassic boundary sections: a complex anoxic event and its relationship to contemporaneous mass extinction. *Geological Society of America Bulletin* **122**, 1265–79.

BRETT, C. E., FERRETTI, A., HISTON, K. & SCHÖNLAUB, H. P. 2009. Silurian sequence stratigraphy of the Carnic Alps, Austria. *Palaeogeography, Palaeoclimatology, Palaeoecology* **279**, 1–28.

BRUMSACK, H.-J. 2006. The trace metal content of recent organic carbon-rich sediments: implications for Cretaceous black shale formation. *Palaeogeography, Palaeoclimatology, Palaeoecology* **232**, 344–61.

BRUNNER, C. A., BEAL, J. M., BENTLEY, S. Y. & FURUKAWA, K. 2006. Hypoxia hotspots in the Mississippi Bight. *Journal of Foraminiferal Research* **36**, 95–107.

CALNER, M. 2008. Silurian global events – at the tipping point of climate change. In *Mass Extinctions* (ed. A. M. T. Elewa), pp. 21–58. Berlin, Heidelberg: Springer-Verlag.

COCKS, L. R. M. 2002. Key Lower Palaeozoic faunas from near the Trans-European Suture Zone. In *Palaeozoic Amalgamation of Central Europe* (eds J. A. Winchester, T. C. Pharaoh & J. Verniers), pp. 37–46. Geological Society of London, Special Publication no. 201.

COCKS, L. R. M. & TORSVIK, T. H. 2005. Baltica from the late Precambrian to mid-Paleozoic times: the gain and loss of a terrane's identity. *Earth-Science Reviews* **72**, 39–66.

CRAMER, B. D. & SALTZMAN, M. R. 2005. Sequestration of ^{12}C in the deep ocean during the early Wenlock (Silurian) positive carbon isotope excursion. *Palaeogeography, Palaeoclimatology, Palaeoecology* **219**, 333–49.

CRAMER, B. D. & SALTZMAN, M. R. 2007. Fluctuations in epeiric sea carbonate production during Silurian positive carbon isotope excursions: a review of proposed paleoceanographic models. *Palaeogeography, Palaeoclimatology, Palaeoecology* **245**, 37–45.

DADLEZ, R., KOWALCZEWSKI, Z. & ZNOSKO, J. 1994. Niektóre kluczowe problemy przedpermskiej tektoniki Polski. *Geological Quarterly* **38**, 169–90.

DECZKOWSKI, Z. & TOMCZYK, H. 1969. Older Palaeozoic in borehole Wilków (Northern Part of the Świętokrzyskie Mountains). *Geological Quarterly* **13**, 14–24. (in Polish with English summary)

DE KOFF, J. P., ANDERSON, M. A. & AMRHEIN, C. 2008. Geochemistry of iron in the Salton Sea, California. *Hydrobiologia* **604**, 111–21.

DÍAZ-MARTÍNEZ, E. & GRAHN, Y. 2007. Early Silurian glaciation along the western margin of Gondwana (Peru, Bolivia and northern Argentina): palaeogeographic and geodynamic setting. *Palaeogeography, Palaeoclimatology, Palaeoecology* **245**, 62–81.

EMSBO, P., MCLAUGHLIN, P., MUNNECKE, A., BREIT, G. N., KOENIG, A. E., JEPPSSON, L. & VERPLANCK, P. L. 2010. The Ireviken Event: a Silurian OAE. *Geological Society of America Abstracts with Programs* **42**(5), 561.

HAMMARLUND, E. U., DAHL, T. W., HARPER, D. A. T., BOND, D. P. G., NIELSEN, A. T., BJERRUM, C. J., SCHOVSBO, N. H., SCHÖNLAUB, H. P., ZALASIEWICZ, J. A. & CANFIELD, D. E. 2012. A sulfidic driver for the end-Ordovician mass extinction. *Earth and Planetary Science Letters* **331–332**, 128–39.

HARPER, D. A. T., HAMMARLUND, E. U. & RASMUSSEN, C. M. Ø. 2014. End Ordovician extinctions: a coincidence of causes. *Gondwana Research* **25**, 1294–307.

HARTZ, E. & TORSVIK, T. H. 2002. Baltica upside down: a new plate tectonic model for Rodinia and the Iapetus Ocean. *Geology* **30**, 255–8.

HATCH, J. R. & LEVENTHAL, J. S. 1992. Relationship between inferred redox potential of the depositional environment

and geochemistry of the Upper Pennsylvanian (Missourian) Stark Shale Member of the Dennis Limestone, Wabaunsee County, Kansas, U.S.A. *Chemical Geology* **99**, 65–82.

JEPPSSON, L. 1990. An oceanic model for lithological and faunal changes tested on the Silurian record. *Journal of the Geological Society, London* **147**, 663–74.

JOHNSON, M. E. 2006. Relationship of Silurian sea-level fluctuations to oceanic episodes and events. *GFF* **128**, 123–9.

JOHNSON, M. E. 2010. Tracking Silurian eustasy: alignment of empirical evidence or pursuit of deductive reasoning? *Palaeogeography, Palaeoclimatology, Palaeoecology* **296**, 276–84.

JONES, B. & MANNING, D. A. C. 1994. Comparison of geochemical indices used for the interpretation of palaeoredox conditions in ancient mudstone. *Chemical Geology* **111**, 111–29.

KALJO, D. & MARTMA, T. 2006. Application of carbon isotope stratigraphy to dating the Baltic Silurian rocks. *GFF* **128**, 123–9.

KOZŁOWSKI, W. 2008. Lithostratigraphy and regional significance of the Nowa Słupia Group (Upper Silurian) of the Łysogóry Region (Holy Cross Mountains, Central Poland). *Acta Geologica Polonica* **58**, 43–74.

KREMER, B. 2005. Mazuelloids: product of post-mortem phosphatization of acanthomorphic acritarchs. *Palaios* **20**, 27–36.

LALLIER-VERGES, E., BERTRAND, P. & DESPRAIRIES, A. 1993. Organic matter composition and sulfate reduction intensity in Oman Margin sediments. *Marine Geology* **112**, 57–69.

LEHNERT, O., MÄNNIK, P., JOACHIMSKI, M. M., CALNER, M. & FRÝDA, J. 2010. Palaeoclimate perturbations before the Sheinwoodian glaciation: a trigger for extinctions during the 'Ireviken Event'. *Palaeogeography, Palaeoclimatology, Palaeoecology* **296**, 320–31.

LOYDELL, D. K. 1998. Early Silurian sea-level changes. *Geological Magazine* **135**, 447–71.

LOYDELL, D. K. 2007. Early Silurian positive $\delta^{13}C$ excursions and their relationship to glaciations, sea-level changes and extinction events. *Geological Journal* **42**, 531–46.

LOYDELL, D. K. & FRÝDA, J. 2007. Carbon isotope stratigraphy of the upper Telychian and lower Sheinwoodian (Llandovery–Wenlock, Silurian) of the Banwy River section, Wales. *Geological Magazine* **144**, 1015–9.

LÜNING, S., KOLONIC, S., LOYDELL, D. K. & CRAIG, J. 2003. Reconstruction of the original organic richness in weathered Silurian shale outcrops (Murzuq and Kufra basins, southern Libya). *GeoArabia* **8**, 299–308.

MALEC, J. 2006. Silurian in the Holy Cross Mountains. In *77th Meeting of the Polish Geological Society, Conference Volume* (eds S. Skompski & A. Żylińska), pp. 36–50 (in Polish).

MARYNOWSKI, L., RAKOCIŃSKI, M., BORCUCH, E., KREMER, B., SCHUBERT, B. A. & JAHREN, A. H. 2011. Molecular and petrographic indicators of redox conditions and bacterial communities after F/F mass extinction. *Palaeogeography, Palaeoclimatology, Palaeoecology* **306**, 1–14.

MARYNOWSKI, L., ZATOŃ, M., RAKOCIŃSKI, M., FILIPIAK, P., KURKIEWICZ, S. & PEARCE, T. J. 2012. Deciphering the upper Famennian Hangenberg Black Shale depositional environments based on multi-proxy record. *Palaeogeography, Palaeoclimatology, Palaeoecology* **346/347**, 66–86.

MCLAUGHLIN, P. A., EMSBO, P. & BRETT, C. E. 2012. Beyond black shales: the sedimentary and stable isotope records of oceanic anoxic events in a dominantly oxic basin (Silurian; Appalachian Basin, USA). *Palaeogeography, Palaeoclimatology, Palaeoecology* **367–368**, 153–77.

MELCHIN, M. J., SADLER, P. M. & CRAMER, B. D. 2012. Chapter 21: The Silurian Period. In *The Geologic Time Scale 2012* (eds F. M. Gradstein, J. G. Ogg, M. Schmitz & G. Ogg), pp. 525–58. New York: Elsevier.

MODLIŃSKI, Z. & SZYMAŃSKI, B. 2001. The Silurian of the Nida, Holy Cross Mts. and Radom areas, Poland – a review. *Geological Quarterly* **45**, 435–54.

MUNNECKE, A., CALNER, M., HARPER, D. A. T. & SERVAIS, T. 2010. Ordovician and Silurian sea-water chemistry, sea level, and climate: a synopsis. *Palaeogeography, Palaeoclimatology, Palaeoecology* **296**, 389–413.

MUNNECKE, A., SAMTLEBEN, C. & BICKERT, T. 2003. The Ireviken Event in the lower Silurian of Gotland, Sweden – relation to similar Palaeozoic and Proterozoic events. *Palaeogeography, Palaeoclimatology, Palaeoecology* **195**, 99–124.

NARKIEWICZ, M. 2002. Ordovician through earliest Devonian development of the Holy Cross Mts. (Poland): constraints from subsidence analysis and thermal maturity data. *Geological Quarterly* **46**, 255–66.

NAWROCKI, J., DUNLAP, J., PECSKAY, Z., KRZEMIŃSKI, L., ŻYLIŃSKA, A., FANNING, M., KOZŁOWSKI, W., SALWA, S., SZCZEPANIK, Z. & TRELA, W. 2007. Late Neoproterozoic to Early Palaeozoic palaeogeography of the Holy Cross Mountains (Central Poland): an integrated approach. *Journal of the Geological Society, London* **164**, 405–23.

NEUMANN, T., RAUSCH, N., LEIPE, T., DELLWIG, O., BERNER, Z., & BOTTCHER, M. E. 2005. Intense pyrite formation under low sulfate conditions in the Achterwasser lagoon, SW Baltic Sea. *Geochimica et Cosmochimica Acta* **69**, 3619–30.

NOBLE, P. J., ZIMMERMAN, M. K., HOLMDEN, CH. & LENZ, A. C. 2005. Early Silurian (Wenlockian) $\delta^{13}C$ profiles from the Cape Phillips Formation, Arctic Canada and their relation to biotic events. *Canadian Journal of Earth Sciences* **42**, 1419–30.

O'BRIEN, N. R. 1996. Shale lamination and sedimentary processes. In *Palaeoclimatology and Palaeoceanography from Laminated Sediments* (ed. A. E. S. Kemp), pp. 23–36. Geological Society of London, Special Publication no. 116.

PAGE, A., ZALASIEWICZ, J., WILLIAMS, M. & POPOV, L. 2007. Were transgressive black shales a negative feedback modulating glacioeustasy in the Early Palaeozoic Icehouse? In *Deep-Time Perspectives on Climate Change: Marrying the Signal from Computer Models and Biological Proxies: Special Publication of the Geological Society of London* (eds. M. Williams, A. M. Haywood, F. J. Gregory, D. N. Schmidt), pp. 123–56. The Micropalaeontological Society.

PODHALAŃSKA, T. & TRELA, W. 2007. Stratigraphy and sedimentary record of the Lower Silurian succession in the southern Holy Cross Mountains, Poland. *Acta Palaeontologica Sinica* **46** (Suppl), 397–401.

POPRAWA, P., ŠLJAUPA, S., STEPHENSON, R. A. & LAZAUSKIENE, J. 1999. Late Vendian–Early Palaeozoic tectonic evolution of the Baltic basin: regional implications from subsidence analysis. *Tectonophysics* **314**, 219–39.

RACKA, M., MARYNOWSKI, L., FILIPIAK, P., SOBSTEL, M., PISARZOWSKA, A. & BOND, D. P. G. 2010. Anoxic *Annulata* Events in the Late Famennian of the Holy Cross Mountains (Southern Poland): geochemical and

https://doi.org/10.1017/S0016756815001065 Published online by Cambridge University Press

palaeontological record. *Palaeogeography, Palaeoclimatology, Palaeoecology* **297**, 549–75.

RACKI, G., BALIŃSKI, A., WRONA, R., MAŁKOWSKI, K., DRYGANT, D. & SZANIAWSKI, H. 2012. Faunal dynamics across the Silurian–Devonian positive isotope excursions ($\delta^{13}C$, $\delta^{18}O$) in Podolia, Ukraine: comparative analysis of the Ireviken and Klonk events. *Acta Palaeontologica Polonica* **57**, 795–832.

RIMMER, S. M. 2004. Geochemical paleoredox indicators in Devonian–Mississipian black shales, Central Appalachian Basin (USA). *Chemical Geology* **206**, 373–91.

ROSS, D. A. & DEGENS, E. T. 1974. Recent sediments of the Black Sea. In *Black Sea – Geology, Chemistry, and Biology* (eds E. T. Degens & D. A. Ross), pp. 183–99. Association of American Petroleum Geologists Memoir 20.

ROSS, C. A. & ROSS, J. P. R. 1996. Silurian sea-level fluctuations. In *Paleozoic Sequence Stratigraphy: Views from the North American Craton* (eds B. J. Witzke, G. A. Ludvigson, J. Day), pp. 187–92. Geological Society of America Special Paper 306.

RUBINOWSKI, Z. 1969. Position of the siderite-pyrite mineralization in the Palaeozoic core of the Holy Cross Mountains. *Annales de la Société Géologique de Pologne* **39**, 721–2 (in Polish).

SAGEMAN, B. B. & LYONS, T. W. 2004. Geochemistry of fine-grained sediments and sedimentary rocks. In *Sediments, Diagenesis, and Sedimentary Rocks; Treatise on Geochemistry, vol. 7* (ed. F. MacKenzie), pp. 115–58. New York: Elsevier.

SCHALLREUTER, R. 1984. Framboidal pyrite in deep sea sediments. In *Initial Reports of the Deep Sea Drilling Project, vol. 75* (eds W. W. Hay, J.-C. Sibuet, E. J. Barron, S. Brassell, W. E. Dean, A.Y. Huc, B. H. Keating, C. L. McNulty, P. A. Meyers, M. Nohara, R. E. Schallreuter, J. C. Steinmetz, D. Stow & H. Stradner), pp. 875–91. Washington, DC: US Government Printing Office.

SCHIEBER, J. 1994. Evidence for episodic high energy events and shallow-water deposition in the Chattanooga Shale, Devonian, central Tennessee. *U.S.A. Sedimentary Geology* **93**, 193–208.

SCHIEBER, J. & SCHIMMELMANN, A. 2006. High resolution pyrite framboid size distribution in Santa Barbara Basin sediments: implications for the study of black shales. *Eos (Transactions, American Geophysical Union)* **87**(36). Ocean Sciences Meeting Supplement, Abstract OS46A-11.

SCHIEBER, J. & SCHIMMELMANN, A. 2007. High resolution study of pyrite framboid distribution in varved Santa Barbara Basin sediments and implications for water-column oxygenation. *Pacific Climate (PACLIM) 2007 Workshop, Asilomar State Beach and Conference Grounds, Pacific Grove, California, May 13–16, 2007* (poster presentation).

SCHIEBER, J., SOUTHARD, J. B. & SCHIMMELMANN, A. 2010. Lenticular shale fabrics resulting from intermittent erosion of water-rich muds – interpreting the rock record in the light of recent flume experiments. *Journal of Sedimentary Research* **80**, 119–28.

SMOLAREK, J., MARYNOWSKI, L., SPUNDA, K. & TRELA, W. 2014. Vitrinite equivalent reflectance of Silurian black shales from the Holy Cross Mountains, Poland. *Mineralogia* **45**, 79–96.

SPENGLER, A. E. & READ, J. F. 2010. Sequence development on a sediment-starved, low accommodation epeiric carbonate ramp: Silurian Wabash Platform, USA mid-continent during icehouse to greenhouse transition. *Sedimentary Geology* **224**, 84–115.

SWANNER, E. D., PLANAVSKY, N. J., LALONDE, S. V., ROBBINS, L. J., BEKKER, A., ROUXEL, O. J., SAITO, M. A., KAPPLER, A., MOJZSIS, S. J. & KONHAUSER, K. O. 2014. Cobalt and marine redox evolution. *Earth and Planetary Science Letters* **390**, 253–63.

TOMCZYK, H. & TOMCZYKOWA, E. 1976. Development of Ashgill and Llandovery sediments in Poland. In *The Ordovician System* (ed. M. Basset), pp. 327–449. Cardiff: University of Wales Press and The National Museum of Wales.

TORSVIK, T. H. & REHNSTRÖM, E. F. 2001. Cambrian palaeomagnetic data from Baltica: implications for true polar wander and Cambrian palaeogeography. *Journal of the Geological Society, London* **158**, 321–9.

TRELA, W. 2006. Lithostratigraphy of the Ordovician in the Holy Cross Mountains. *Przegląd Geologiczny* **54**, 622–31 (in Polish with English summary).

TRELA, W. & SALWA, S. 2007. Litostratygrafia dolnego syluru w odsłonięciu Bardo Stawy (południowa część Gór Świętokrzyskich): związek ze zmianami poziomu morza i cyrkulacją oceaniczną;. *Przegląd Geologiczny* **55**, 971–78.

TRIBOVILLARD, N., ALGEO, T. J., LYONS, T. & RIBOULLEAU, A. 2006. Trace metals as paleoredox and paleoproductivity proxies: an update. *Chemical Geology* **232**, 12–32.

VANDENBROUCKE, T. R. A., MUNNECKE, A., LENG, M. J., BICKERT, T., HINTS, O., GELSTHORPE, D., MAIER, G. & SERVAIS, T. 2013. Reconstructing the environmental conditions around the Silurian Ireviken Event using the carbon isotope composition of bulk and palynomorph organic matter. *Geochemistry Geophysics Geosystems* **14**, 86–101.

WANG, L., SHI, X. & JIANG, G. 2012. Pyrite morphology and redox fluctuations recorded in the Ediacaran Doushantuo Formation. *Palaeogeography, Palaeoclimatology, Palaeoecology* **333–334**, 218–27.

WIGNALL, P. B. 1991. Test of the concepts of sequence stratigraphy in the Kimmeridgian (Late Jurassic) of England and northern France. *Marine & Petroleum Geology* **8**, 430–41.

WIGNALL, P. B. 1994. *Black Shales*. Oxford: Clarendon Press.

WIGNALL, P. B., BOND, D. P. G., KUWAHARA, K., KAKUWA, Y., NEWTON, R. J. & POULTON, S. W. 2010. An 80 million year oceanic redox history from Permian to Jurassic pelagic sediments of the Mino-Tamba terrane, SW Japan, and the origin of four mass extinctions. *Global and Planetary Change* **71**, 109–23.

WIGNALL, P. B. & MAYNARD, J. R. 1993. The sequence stratigraphy of transgressive black shales. *American Association of Petroleum Geologists Studies in Geology* **37**, 35–47.

WIGNALL, P. B. & NEWTON, R. 1998. Pyrite framboid diameter as a measure of oxygen-deficiency in ancient mudrocks. *American Journal of Science* **298**, 537–52.

WILDE, P., BARRY, W. B. N. & QUINBY-HUNT, M. S. 1991. Silurian oceanic and atmospheric circulation and chemistry. *Special Papers in Palaeontology* **44**, 123–43.

WILKIN, R. T. & ARTHUR, M. A. 2001. Variations in pyrite texture, sulfur isotope composition, and iron systematics in the Black Sea: Evidence for Late Pleistocene to Holocene excursions of the O_2–H_2S redox

https://doi.org/10.1017/S0016756815001065 Published online by Cambridge University Press

transition. *Geochimica et Cosmochimica Acta* **65**, 1399–416.

WILKIN, R. T., BARNES, H. L. & BRANTLEY, S. L. 1996. The size distribution of framboidal pyrite in modern sediments: an indicator of redox conditions. *Geochimica et Cosmochimica Acta* **60**, 3897–912.

ZHOU, CH. & JIANG, S.-Y. 2009. Palaeoceanographic redox environments for the lower Cambrian Hetang Formation in South China: evidence from pyrite framboids, redox sensitive trace elements, and sponge biota occurrence. *Palaeogeography, Palaeoclimatology, Palaeoecology* **271**, 279–86.

ZHOU, L., WIGNALL, P. B., SU, J., FENG, Q., XIE, S., ZHAO, L. & HUANG, J. 2012. U/Mo ratios and $\delta^{98}/^{95}$Mo as local and global redox proxies during mass extinction events. *Chemical Geology* **324–325**, 99–107.

https://doi.org/10.1017/S0016756815001065 Published online by Cambridge University Press